Springer

Acta Mechanica Sinica

CrossMark click for updates

•RESEARCH PAPER•

Acta Mech. Sin., Vol. 38, 321363 (2022)
https://doi.org/10.1007/s10409-022-21363-x

Aerodynamic optimization using passive control devices near the bogie cabin of high-speed trains

Yongfang Yao[1,2], Zhenxu Sun[1*], Guibo Li[3], Guowei Yang[1,2], Prasert Prapamonthon[4], Yi Guo[1], and Mengying Wang[1,2]

[1] *Key Laboratory for Mechanics in Fluid Solid Coupling Systems, Institute of Mechanics, Chinese Academy of Sciences, Beijing 100190, China;*
[2] *School of Engineering Sciences, University of Chinese Academy of Sciences, Beijing 100049, China;*
[3] *China Railway Rolling Stock Corporation Qingdao Sifang Co., Ltd., Qingdao 266111, China;*
[4] *International Academy of Aviation Industry, King Mongkut's Institute of Technology Ladkrabang, Bangkok 10520, Thailand*

Received July 23, 2021; accepted September 6, 2021; published online May 26, 2022

Bogies are responsible for a significant amount of aerodynamic resistance and noise, both of which negatively affect high-speed train performance and passenger comfort. In the present study, the passive control method is applied in designing the bogie cabins of a high-speed train to improve its aerodynamic characteristics. Two passive control measures are introduced, namely, adding a spoiler and creating diversion grooves near the bogie cabins. Furthermore, the aerodynamic and aeroacoustic characteristics of a high-speed train operating at 350 km/h under different control strategies are numerically investigated using the improved-delayed-detached-eddy simulation (IDDES) and the acoustic finite element method (FEM). The impacts of passive control devices on drag reduction, slipstream, and aerodynamic noise are presented and discussed. Numerical results reveal that the passive control devices have a major effect on the slipstream around the train. The amplitude of the fluctuating pressure is higher in the first half of the train than in the second half. The first bogie has the maximum amplitude of the acoustic pressure for both the train with and without passive devices. In the far field, the spoiler installation and placement of the diversion grooves in the front of the bogie cabin can significantly reduce aerodynamic drag and noise. Hence, as shown in this study, using passive control methods to improve the aerodynamic and aeroacoustic properties of high-speed trains can be a viable option.

Passive control devices, Aerodynamic drag, Slipstream, Aerodynamic noise, High-speed trains

Citation: Y. Yao, Z. Sun, G. Li, G. Yang, P. Prapamonthon, Y. Guo, and M. Wang, Aerodynamic optimization using passive control devices near the bogie cabin of high-speed trains, Acta Mech. Sin. **38**, 321363 (2022), https://doi.org/10.1007/s10409-022-21363-x

1. Introduction

Bogie, which is an important component of high-speed trains, can significantly affect vehicle stability, train aerodynamics, and passenger comfort. For high-speed trains, the aerodynamic resistance includes friction and pressure drag. To increase the performance of the high-speed trains, the reduction of the train resistance is considered by decreasing the friction and pressure drag. Raghunathan et al. [1] found that bogies contributed approximately 38%-47% of the aerodynamic drag when a high-speed train ran at cruise speed. Therefore, designing and optimizing the bogies and structures around them to reduce aerodynamic drag seems promising. Consequently, the performance of the train can be improved.

Flow control (including active control and passive control) can be used in designing the bogie cabin and bogie skirt. The frequently used passive control devices include vortex generators, wall microstructures, surface coating materials, and flexible walls. Compared with the active control methods, the passive control approach is simpler and does not require additional energy. Moreover, the passive control approach has lower design and manufacturing costs. The active control method is effective in running structures with complex motion postures, whereas passive control has a wider scope of applications because it is simple and effective. Recently,

*Corresponding author. E-mail address: sunzhenxu@imech.ac.cn (Zhenxu Sun)
Executive Editor: Xuesong Wu

several types of research on the flow control of the aerodynamic noise of the bomb bay have been conducted. The improved separation characteristics of the embedded weapons in the aviation field, such as the leading edge and spoiler, are applied to the F-22 and B-2 aircraft. Vakili et al. [2,3] studied the noise suppression effect of adding horizontal or vertical spoiler bars in front of a missile cabin using wind tunnel tests and numerical simulations and discovered that the distribution and shape of spoiler bars are important factors affecting the noise suppression level. However, the motion and change of track attitude of a high-speed train are much smaller than those of the aircraft. Therefore, it is feasible to adopt passive control methods to improve the aerodynamic and aeroacoustic performance of high-speed trains.

Recently, several groups of researchers have used experimental and/or numerical approaches to study the drag-reduction technology of the bogie system and the corresponding flow characteristics at the bottom of the train. For example, based on the study of several models of the Shinkansen line in Japan, the influence of the installation of a bogie rectifying device on the aerodynamics of the flow field around electric multiple units (EMU) was reported [4]. Baker [5] detected the operation parameters of the ETR500 train through a wind tunnel test and concluded that the bogie rectifier device could reduce the aerodynamic resistance of high-speed trains. Studies by Ido et al. [6] revealed that the airflow at the bottom of the train was sensitive to the shape of the bottom of the train. Wang et al. [7] investigated the effects of bogies on high-speed train slipstream and wake. They concluded that the bogies increased the wake's turbulence level and slipstream velocity. Huang et al. [8] studied the drag-reduction performance of a three-group train model equipped with a diversion structure at the rear of the bogie carriage. However, as the two-way operation characteristics of the train are not considered here, certain problems still exist with the application. With the recent capability of computer performance, numerical approaches have been used for the aerodynamic analysis of high-speed trains. According to Kaltenbach et al. [9], the bogie configuration alters the underbody flow. Yang et al. [10] showed that the installation of an apron board at the bottom of the train reduced the aerodynamic resistance of the train. The most effective way of installing an apron on the bogie at the end of the first and last car was introduced. Wang et al. [11] studied EMU running at 350 km/h and concluded that the running resistance of the train could be reduced by adding a side apron board. Zheng et al. [12] analyzed the influence of the end baffle and diversion structure on the bogie resistance of the head and tail carriages and pointed out that the improvement of the bottom structure reduced the aerodynamic resistance of the bogie. Chen et al. [13] designed four types of deflectors for bogies: straight, inclined, inner arc, and outer arc. Their results showed that the difference in the total resistance of the trains with different bottom deflectors could reach 20%. The straight guide deflectors performed the best at reducing the aerodynamic resistance. The study by Wang et al. [14] showed that the bogies covered by full-size bogie fairings significantly reduced the train slipstream velocity, and larger bogie fairings were recommended to improve the safety of roadside workers and passengers standing on the platform.

In addition, it is obvious that the sound produced by running high-speed trains is likely to disturb passengers and nearby communities, and many researchers have proposed that bogie is an important source of aerodynamic noise [15-22]. To alleviate this problem, the effects of aerodynamic noise and the influence of bottom structures, such as bogies, on aerodynamic noise production have been experimentally and numerically studied [23-30]. Frémion et al. [23] tested the aerodynamic noise at the connection part of a vehicle and the bogie of a TGV in France. They discovered that the noise in the bogie area comprised various incoherent sound sources, and the formation mechanism was complex. Torii and Ito [24] investigated the effects of the apron board installed on the bogie part of the 700 series Shinkansen train and found that the interaction between the air and the bogie area could be improved. They also found that the formation and propagation of the aerodynamic noise could be reduced. Huang et al. [25] conducted a numerical simulation of the aerodynamic noise on the bogie of a high-speed train. The results showed that the aerodynamic noise at the bogie was broadband noise. By optimizing the design of the bogie outer skirt, the aerodynamic noise was reduced. Zhang et al. [26] analyzed the far-field aerodynamic noise of the train and the aerodynamic performance of the main components in the bogie cabin. Zhu et al. [27] analyzed the influence of the bogie cabin on the bogie flow and aeroacoustic characteristics. The results indicated that the bogie cabin changes the flow characteristics and sound radiation directivity of the bogie. The aerodynamic noise produced by the bogie can be reduced; however, the rear wall of the bogie cabin produces greater aerodynamic noise. Furthermore, studies conducted by Lauterbach et al. [28-30] also indicated that the installation of an apron board was effective in mitigating the turbulent motion and flow impact of bogie components. Consequently, the resistance and aerodynamic noise of the bogie components were reduced.

Moreover, better aerodynamic characteristics can be obtained by optimizing the bogie region of the high-speed trains. The drag reduction can be achieved through the shape design of the bogie cabin, such as changing the shape of the transition from bottom to top or using different coatings on the outside of the bogie cabin. To date, most previous studies have only considered the effects of drag reduction, yet few studies have focused on aerodynamic noise reduction. The influence of the drag reduction strategy on outdoor noise

needs to be further explored. Therefore, this study aims to numerically investigate the effects of using passive control devices near the bogie cabin of a high-speed train on drag and noise reduction. Two kinds of passive control methods, adding a spoiler and setting diversion grooves, are applied to the bogie region to investigate the flow field and sound field. The remainder of this study is organized as follows. Computational models and methods are presented in Sects. 2 and 3, respectively. The results and discussion are given in Sect. 4. The conclusion and some remarks are drawn in Sect. 5.

2. Computational models

A three-grouped train model with a pantograph and bogies is adopted for numerical simulation. To study drag and noise reduction using passive control devices near the bogie cabin, the regions near the bogie cabins of the baseline model are modified by adding diversion grooves or adding a spoiler, as shown in Fig. 1a-c, respectively. Figure 1a shows the side and bottom views of the baseline shape, which is named Configuration 1. The passive control devices are added in front of the bogie cabin to achieve new computational models. The models with passive control devices, namely, adding diversion grooves and adding a spoiler, are named Configuration 2 and Configuration 3, respectively. Figure 1b shows the size of the diversion grooves added in configuration 2, specifically, the longest side L = 656 mm, height H = 140 mm, angle between the short slope and the vehicle ground θ = 56º, and distance between the triangle position and the bogie cabin D = 0 mm, indicating that it is closely connected to the bogie cabin. Figure 1c shows the dimension of the spoiler added in Configuration 3. It extends to 200 mm in front of the cabin along the x-direction and transits 87.8 mm to the ground in the z-direction, and the transverse width y = 2353 mm. The size of the spoiler is $x \times y \times z$ = 200 mm × 2353 mm × 87.8 mm,. Figure 1d shows the geometry of the bogie in the top and bottom views.

3. Computational methods

3.1 Numerical algorithms for CFD

Here, the numerical approach of the improved-delayed-detached-eddy simulation (IDDES) is used in the numerical simulation to obtain unsteady flow details. The IDDES

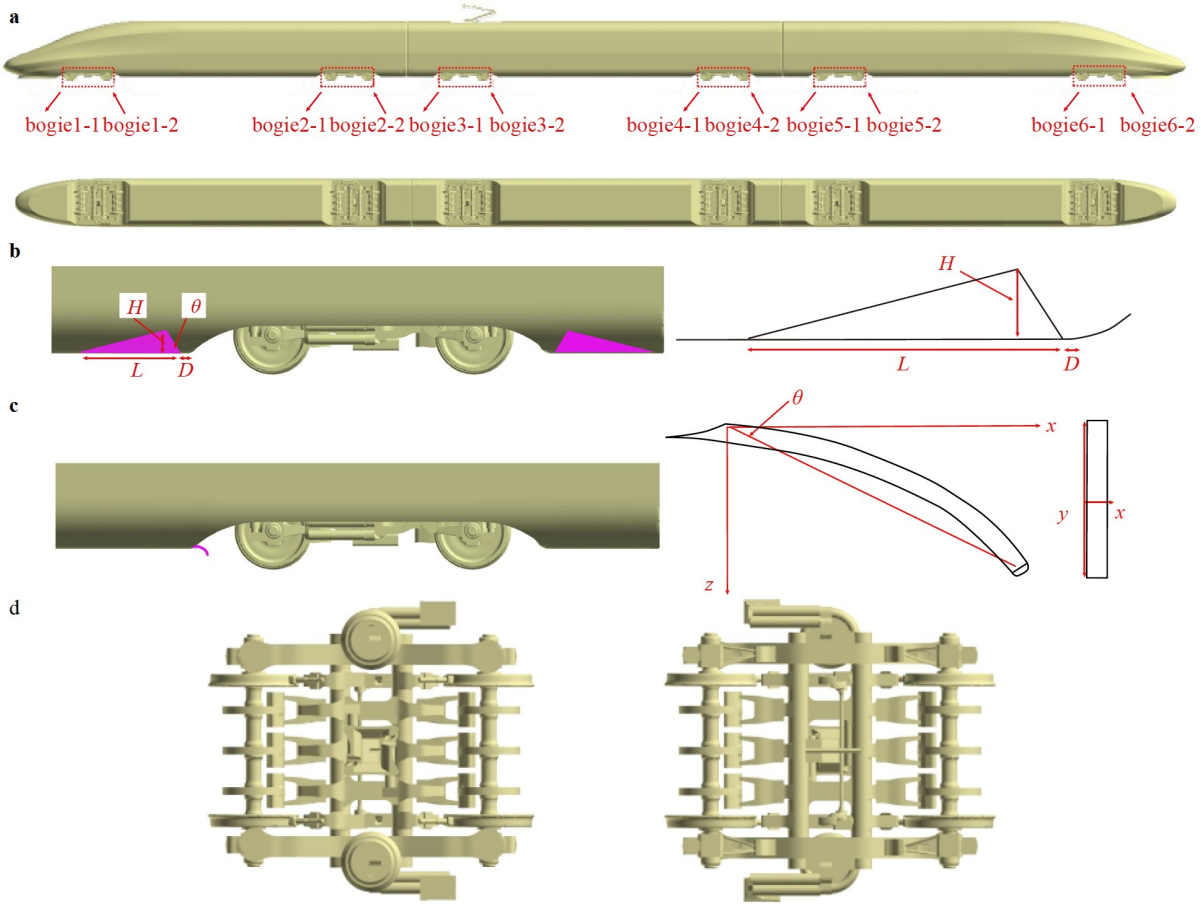

Figure 1 Train models: **a** side and bottom views of the baseline train model with bogies (Configuration 1), **b** adding diversion grooves and their dimensions (Configuration 2), **c** adding a spoiler and their dimensions (Configuration 3), and **d** top and bottom views of the bogie.

method was developed from the detached-eddy simulation (DES) proposed by Spalart et al. [31]. The DES approach combines the large eddy simulation (LES) and the Spalart-Allmaras (SA) model. It can automatically switch between the two methods by comparing the local-grid scale and wall distance. In 2006, Spalart et al. [32] developed the delayed-detached-eddy simulation (DDES) using the "Delay LES Function" based on the idea [33] of Menter's SST k-w model. The DDES method uses the delay function to protect the boundary layer and avoids the mesh-induced separation problem in the original DES method. However, it causes the log-layer mismatch (LLM) phenomenon. To suppress the LLM problem, Shur et al. [34] proposed the IDDES by introducing a lifting function, f_e, and a branch of wall modeled LES (WMLES). The IDDES can be the DDES when the boundary layer grids are sparse. When the boundary layer grids are dense, the IDDES can be automatically switched to the WMLES, which greatly broadens the scope of applications of the method.

Recently, IDDES simulations have been used in engineering applications, such as train aerodynamics (Dong et al. [35-37]). Thus, in this study, the IDDES method is also used to investigate the effects of the passive control method on the aerodynamic performance of a high-speed train. Based on the principle of the IDDES method, the definitions of L_{RANS} and L_{LES} are the same as those of the DDES, which take the form of

$$\begin{aligned} L_{\mathrm{RANS}} &= \sqrt{k}\,/\left(C_{\mu}\omega Re_{\infty}\right), \\ L_{\mathrm{LES}} &= C_{\mathrm{DES}}\Delta. \end{aligned} \tag{1}$$

However, the definition of Δ needs to be modified:

$$\Delta = \min\left[\max\left(C_w d_w, C_w \Delta_{\max}\right), \Delta_{\max}\right], \tag{2}$$

$$\begin{aligned} \Delta_{\max} &= \max\left(\Delta_i, \Delta_j, \Delta_k\right), \\ \Delta_{\min} &= \min\left(\Delta_i, \Delta_j, \Delta_k\right), \end{aligned} \tag{3}$$

where $C_w = 0.15$. In the calculation of the high Reynolds number, the normal grid size near the wall is smaller than that in the other two directions, so the value of Δ near the wall is taken as $C_w\Delta_{\max}$. In both configurations, Δ increases to $\Delta_{\max}$, and the definition of Δ degenerates to the DDES. Evidently, IDDES reduces the length scale in the boundary layer, thus reducing the local modular viscosity, which is conducive for the flow instability and turbulence generation in the WMLES branch. The mixed length scale definition of the IDDES introduces the f_e:

$$L_{\mathrm{IDDES}} = \tilde{f}_d\left(1+f_e\right)L_{\mathrm{RANS}} + \left(1-\tilde{f}_d\right)L_{\mathrm{LES}}. \tag{4}$$

The main function of f_e is to increase the modular viscosity of the RANS region in the WMLES branch to avoid the LLM phenomenon in the partition of RANS and LES. For the IDDES method based on the SST model, f_e does not affect the flow [38]. f_d is a delay function, which includes the transition function of the DDES and WMLES branches. Therefore, their expressions are given as

$$f_e = f_{e2}\cdot\max\left[\left(f_{e1}-1\right), 0\right], \tag{5}$$

$$\tilde{f}_d = \max\left[\left(1-f_{dt}\right), f_b\right]. \tag{6}$$

Other functions are constructed as follows:

$$f_{dt} = 1.0 - \tanh\left[\left(C_{dt1}r_{dt}\right)^{C_{dt2}}\right], \tag{7}$$

$$f_b = \min\left[2\exp\left(-9a^2\right), 1\right], \tag{8}$$

$$f_{e1} = \begin{cases} 2\exp(-11.09a^2), & a \geq 0, \\ 2\exp(-9a^2), & a < 0, \end{cases} \tag{9}$$

$$f_{e2} = 1 - \max\left(f_t, f_l\right), \tag{10}$$

$$f_t = \tanh\left[\left(C_t^2 r_{dt}\right)^3\right], \tag{11}$$

$$f_l = \tanh\left[\left(C_l^2 r_{dl}\right)^{10}\right]. \tag{12}$$

Among them,

$$r_{dt} = \frac{\nu_t}{\kappa^2 d_w^2 \sqrt{0.5\left(S^2+\Omega^2\right)}}, \tag{13}$$

$$r_{dl} = \frac{\nu}{\kappa^2 d_w^2 \sqrt{0.5\left(S^2+\Omega^2\right)}}, \tag{14}$$

$$a = 0.25 - d_w/\Delta_{\max}. \tag{15}$$

Here, S is the magnitude of the strain rate tensor, and Ω is the magnitude of the vorticity tensor. The constants $C_{dt1} = 20$, $C_{dt2} = 3$, $C_l = 5$, and $C_t = 1.87$. The function f_b is a transition function in the branch of the WMLES related to the mesh and geometry, which ensures that the thin layer near the wall ($f_b = 1.0$) is a RANS region and switches to the LES region ($f_b = 0$) along the normal direction of the wall. When there is no turbulence in the upstream flow, the Reynolds stress is modeled by RANS, and r_{dt} is greater than 1; thus, $1-f_{dt} > f_b$, and $f_e = 0$. At this time, the length scale of the IDDES becomes

$$L_{\mathrm{IDDES}} \approx L_{\mathrm{DDES}} = \left(1-f_{dt}\right)L_{\mathrm{RANS}} + f_{dt}L_{\mathrm{LES}}. \tag{16}$$

Currently, the IDDES degenerates into the DDES method. When the upstream flow has turbulence pulsation (i.e., the upstream flow is analytical), the modulus of the eddy viscosity is small, and r_{dt} is less than 1; thus, $1-f_{dt} < f_b$. At this time, the length scale of the IDDES becomes

$$\begin{aligned} L_{\mathrm{IDDES}} &\approx L_{\mathrm{WMLES}} \\ &= f_b\left(1+f_e\right)L_{\mathrm{RANS}} + \left(1-f_e\right)L_{\mathrm{LES}}. \end{aligned} \tag{17}$$

In the RANS to LES transition region, $0 < f_b < 1$, $f_e = 0$, the IDDES switches to the WMLES branch.

3.2 Numerical algorithms for acoustics

The acoustic finite element method (FEM) is adopted here to simulate the sound field. This method takes the reflection effect of the surface of the car-body structure on the noise [39] into consideration. The step of the acoustic FEM method starts by calculating the noise propagation from the Helmholtz equation, which takes the following form:

$$\nabla^2 p(x,y,z) - k^2 p(x,y,z) = -j\rho_0 \omega q(x,y,z), \tag{18}$$

where $p(x,y,z)$ is the acoustic pressure, $q(x,y,z)$ is the volume velocity per unit volume, $k = 2\pi f / c$ is the wavenumber, and f is the frequency. The corresponding wavelength is computed from

$$\lambda = 2\pi / k = 2\pi c / \omega = c / f. \tag{19}$$

Then, the fast Fourier transform (FFT) method is adopted for spectral analysis. The square of the amplitude of the pressure wave is expressed as

$$\begin{aligned} A^2(\omega_k) = 2\left[\frac{1}{N}\sum_{n=1}^{N-1}(p_n - \overline{p})\cos\left(\frac{2\pi nk}{N}\right)\right]^2 \\ +2\left[\frac{1}{N}\sum_{n=1}^{N-1}(p_n - \overline{p})\sin\left(\frac{2\pi nk}{N}\right)\right]^2, \end{aligned} \tag{20}$$

where p_n is a data set and represents the fluctuating pressure of the N-th step; $n = 0, 1, \cdots, N-1$. Meanwhile, $\omega_k = k / N\delta t$, where δt is the time step. Finally, the sound pressure level (SPL) is computed by

$$\mathrm{SPL}(\omega_k) = 10\log\left(A^2 / P_{\mathrm{ref}}^2\right), \tag{21}$$

where P_{ref} is constant and equals 2×10^{-5} Pa.

3.3 Boundary conditions and meshing strategy

The computational domain with a size of $66.5H \times 45H \times 20H$ is depicted in Fig. 2a, where H is the height of the train (3.55 m). The inflow velocity is 350 km/h, which corresponds to the Reynolds number, $Re = 2.25 \times 10^7$. The boundary conditions are set as follows. (1) The surface of the train is a fixed wall with no-slip wall conditions. (2) The ground is set to be a moving wall, and its velocity is the same as the incoming velocity of the air. (3) The other boundaries are given as free stream conditions.

Figure 2b and c shows the locations of the monitoring points used to assess the aerodynamic characteristics of the train and the spectrum of sound pressure in near and far fields. Different positions in the x-direction located at x = −60, −50, −40, −30, −20, −10, 0, 10, 20, 30, 40, 50, and 60 m

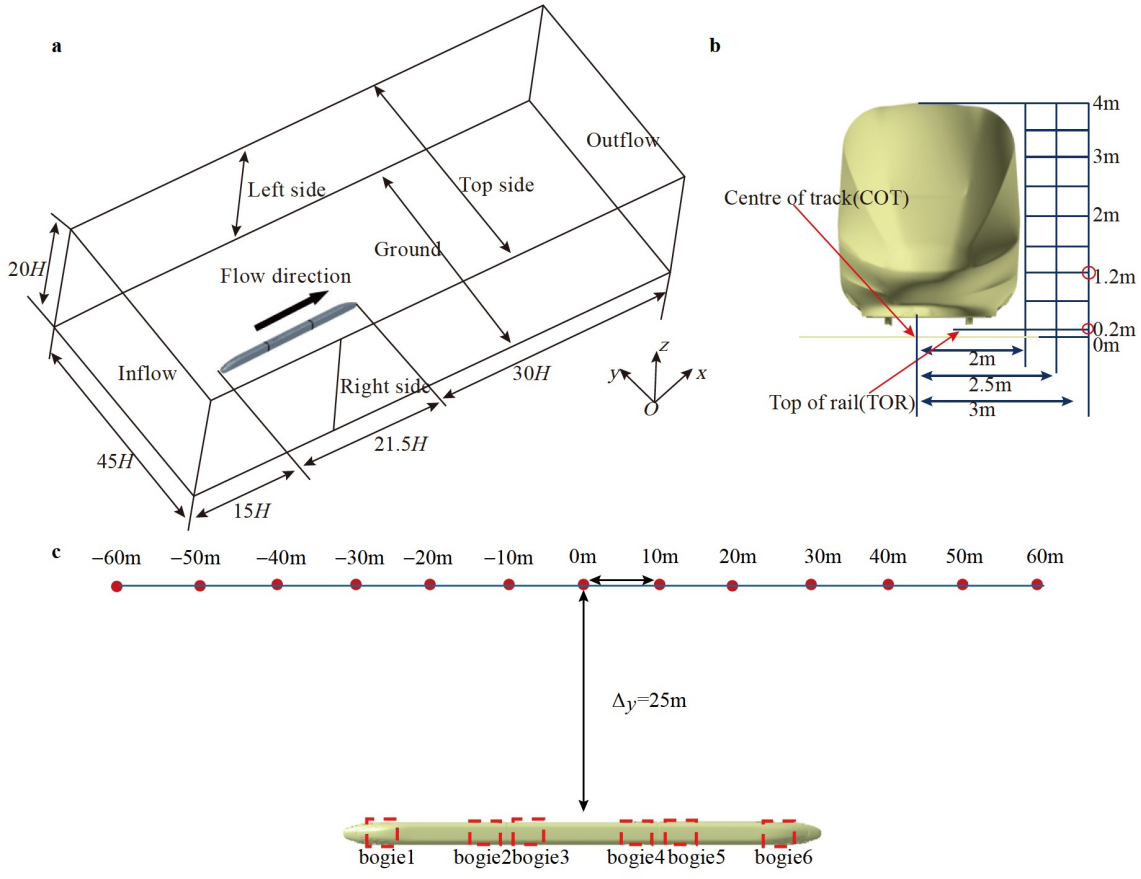

Figure 2 Computational domain for the field and locations of aerodynamic noise observers. **a** Computational domain. **b** Front view of the observers. **c** Top view of the observers.

along the train are monitored to study the overall SPL (OASPL) caused by the train with different passive control devices. Note that these positions are 3.5 m above the ground.

3.4 Numerical validation

First, the mesh independence is validated to acquire sufficiently reliable and accurate numerical results. Afterward, the validation of algorithms for aerodynamic and aeroacoustic computations is presented.

3.4.1 Mesh independence validation

The commercial software STAR-CCM + 9.06 is used for mesh generation. Cartesian grids are generated for the volume mesh, and prism grids are generated near the train surface. The standard wall function is used to reduce the computational grids. Ten layers of prism grids are generated with an increasing ratio of 1.1, which keeps the value of $y+$ of the first layer near the train surface at approximately 30. The grid sizes on the pantograph and bogie surface are 10 and 60 mm, respectively. As shown in Fig. 3, the regions around the train are locally densified. Four mesh refinement zones, including small, middle, large, and wake regions, are set up. Three grid configurations (coarse, medium, and fine grids) are used for the grid-independence study. The total elements of the three numbers are 32, 52, and 72 million for the coarse, medium, and fine grids, respectively. The mesh size of each refinement zone is depicted in Table 1.

According to the grid-independence study, the distributions of the time-averaged slipstream velocity and pressure coefficient along the sampling line at a distance of 2 m from the center of the train, 1.2 m above the ground, obtained from the coarse, medium, and fine meshes are compared, as shown in Fig. 4.

Here, note that the nondimensional slipstream velocity U' is computed from Eq. (22).

$$U' = \sqrt{(V_x - V_\infty)^2 + V_y^2 + V_z^2} / V_\infty, \tag{22}$$

where V_x, V_y, and V_z are the velocity components along the x-, y-, and z-directions, respectively, as shown in Fig. 1, and the nondimensional pressure coefficient C_p' is defined by Eq. (23).

$$C_p' = (p - p_\infty) / \frac{1}{2}\rho_\infty V_\infty^2, \tag{23}$$

where p is the time-averaged surface pressure, p_∞ is the reference pressure, ρ_∞ is the density of incoming flow, and V_∞ is the incoming velocity.

The results obtained from the coarse grid are unacceptable, especially in the rear part of the middle car, whereas the medium and fine grids are close to each other with a maximum error of the time-averaged slipstream velocity of approximately 5%. Therefore, the medium grid (Fig. 5) is selected as the computational grid for all simulations of the flow and sound fields.

3.4.2 Algorithm validation

To validate the accuracy of the numerical approach, simulation results are compared with experimental data. Since the

Table 1 The mesh size of the refinement zones

Grids	Grid configurations (small, middle, big, wake) (mm)	Total amount (million)
Coarse	12, 24, 36, 12	32
Medium	6, 12, 24, 6	52
Fine	6, 9, 18, 6	72

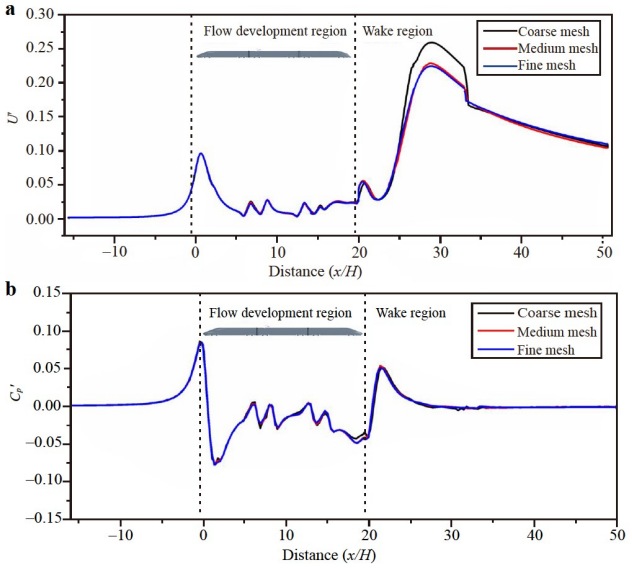

Figure 4 **a** Distribution of the time-averaged slipstream velocity and **b** pressure coefficient along the sampling line obtained from different meshes for the grid-independence study.

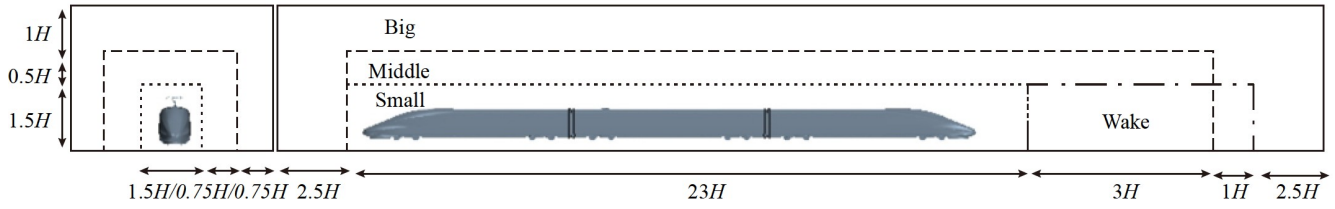

Figure 3 Distribution of refinement zones.

experimental data are obtained using a 1:8 scaled moving model, the numerical simulation model, as shown in Fig. 6a, used for verification is also a 1:8 scaled model. The computational grid and its distribution and refinement zones of the 1:8 scaled model are displayed in Fig. 5. Figure 6b shows the comparison between the pressure distribution predicted by the IDDES simulation and that obtained from the experiments. The time-averaged slipstream is compared in Fig. 6c. The nondimensional results of the slipstream velocity are defined by Eq. (1). The monitoring points in the IDDES simulation are identical to the experiments; they are at a position of 0.375 m from the center of the track (COT) and 0.025 m from the top of the rail. The IDDES simulations provide acceptable results compared with the experimental data, indicating that the IDDES can be used for the simulations in this study. The feasibility of the acoustic FEM for noise analysis was validated previously by Yao et al. [40,41].

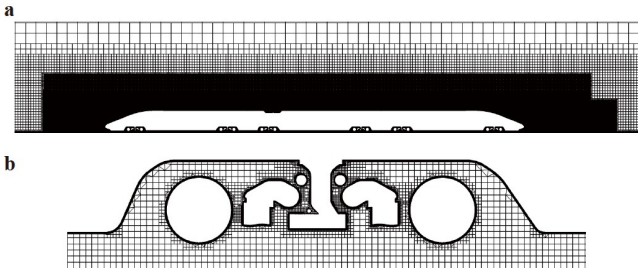

Figure 5 Computational grid and distribution of refinement zones for the medium grid: **a** mesh distribution at plane $y = 0$ and **b** close-up of the mesh distribution around the bogie.

4. Results and discussion

4.1 Analysis of the extreme influence of bogies

The passive control device moderates the flow circumstances around the bogies under the train body. Therefore, the extreme condition is proposed here in advance to determine how the aerodynamic performance could be without bogies. Here, this simplified model is named Configuration 0, and its geometric shape is shown in Fig. 7.

In this section, the aerodynamic resistance and noise generation obtained from a train without bogies are compared with those obtained from a train with bogies, which is named Configuration 1. The influence of the bogies on drag reduction is discussed through the nondimensional coefficient of aerodynamic drag, C_d, which is defined below:

$$C_d = F_d / 0.5\rho U^2 S_{ref}. \tag{24}$$

Here, F_d represents the drag force, ρ denotes the air density with a constant value of 1.225 kg/m^3, and S_{ref} is the reference area (the frontal area with a size of 11.94 m^2 is taken for this study). As shown in Table 2, two kinds of drag coefficients (pressure ($C_{d,p}$) and frictional ($C_{d,f}$) drag coefficients) obtained from the typical train without bogies (Configuration 0) and with bogies (Configuration 1) are compared. Although the train with the bogies gives a lower $C_{d,f}$ than the

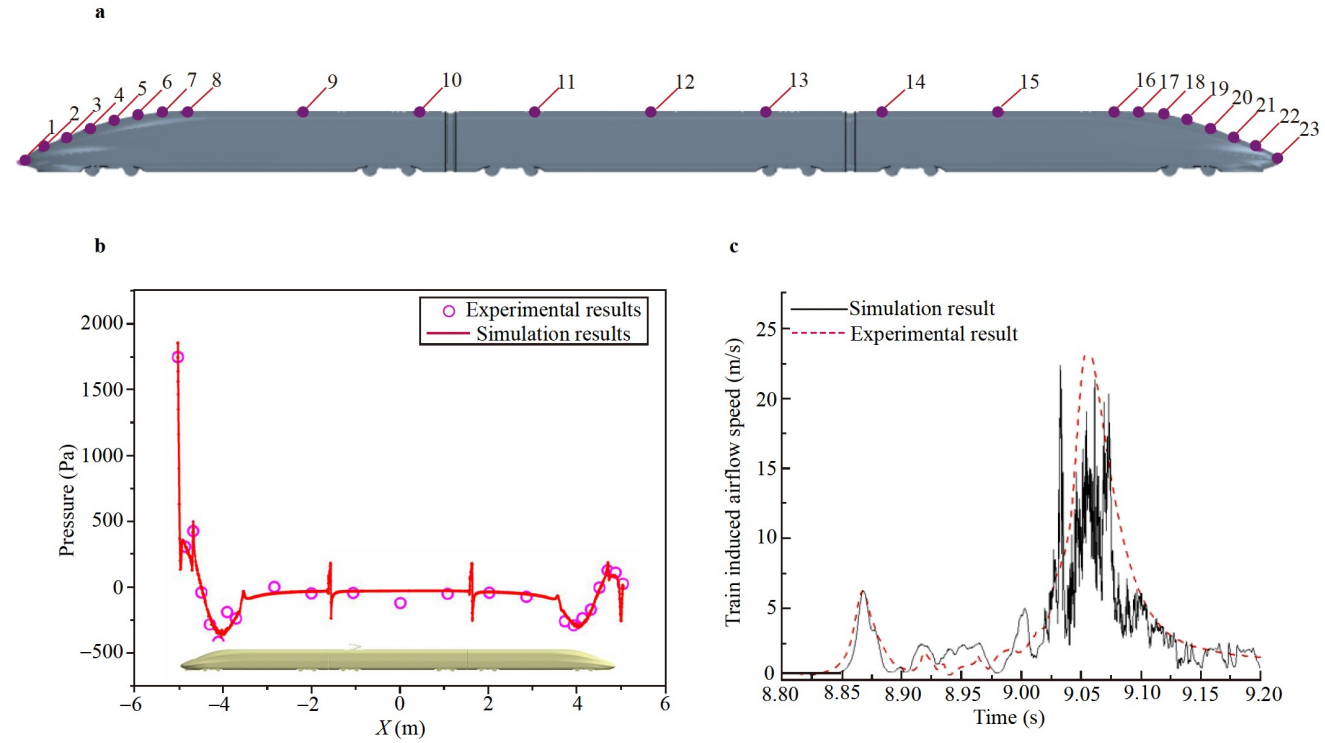

Figure 6 Comparison of distributions of surface pressure and time-averaged slipstream obtained by simulation and experiment: **a** monitoring points, **b** surface pressure distribution, and **c** time-averaged slipstream.

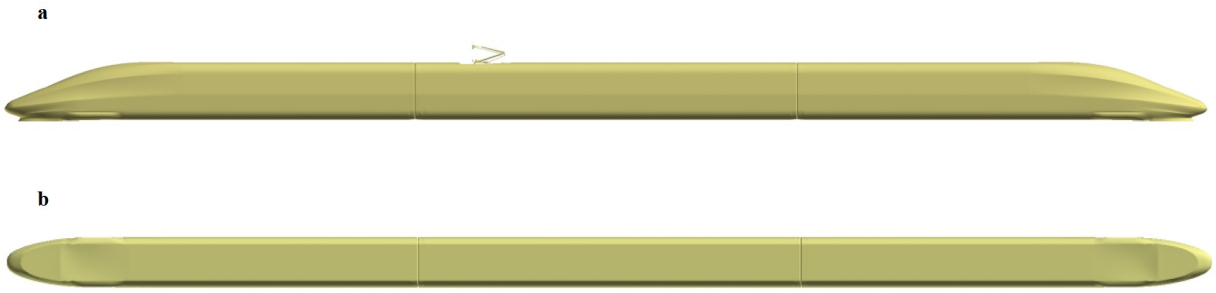

Figure 7 Train shape without bogies in the limit state: **a** lateral view, **b** bottom view.

Table 2 Effect on drag reduction for different train models

Configurations/Drag coefficient	$C_{d,p}$	$C_{d,f}$	$C_{d,total}$	Percentage change
0	0.0616	0.1339	0.1955	–
1	0.2197	0.1111	0.3308	40.9%

train without the bogies, the train with the bogies causes a 40.9% higher $C_{d,total}$ than the train without the bogies, which indicates that the resistance greatly increases due to the presence of the bogie cabins and bogies.

A standard observed probe is set for an aerodynamic noise comparison, positioned 25 m away from the train axis and 3.5 m high from the ground. This probe is located in the middle of the train in the x-direction. Figure 8 shows the sound spectra of the probe generated by the train with and without bogies. The SPL increases to a certain level with the existence of bogies at all frequencies, indicating that the incoming flow is disturbed by the bogies, and the pressure fluctuations near the bogie regions are strengthened. Moreover, the results indicate that the presence of bogies causes a 15 dB higher SPL amplitude than the train without bogies in terms of total SPL. Therefore, the flow control of the bogie regions is essential for reducing drag and noise.

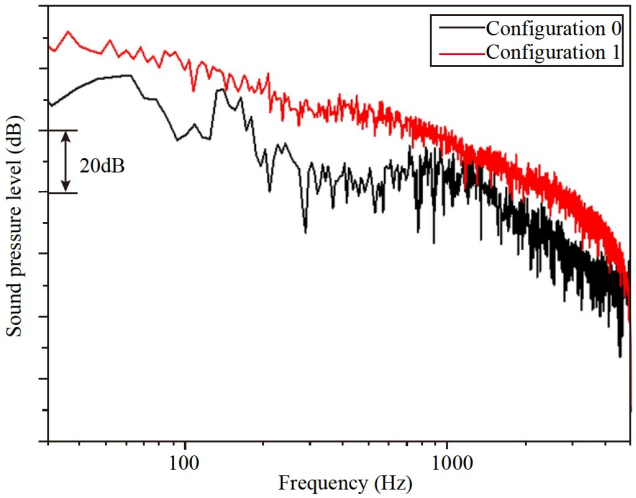

Figure 8 Sound spectrum generated by the train with and without bogies at the middle of the three-grouped train along the x-direction, with y = 25 m and z = 3.5 m..

4.2 Effect of passive control devices on drag reduction

This section presents the effects of passive control devices on the drag reduction of the train. Understanding and predicting the flow around the blunt body is of great engineering significance to guide the design of vehicles, which attracts massive attention in recent years [42]. Flow structures of Configurations 0-3 are depicted by iso-surfaces of instantaneous vortices with a Q-criterion of 1000, as shown in Fig. 9a-d, respectively, to gain a better understanding of these effects. The geometric features and corresponding names are given in Table 3.

In the absence of the train's bogies and bogie cabins, vortices generated by the bogies and bogie cabins on both sides are not formed in Configuration 0, as shown in Fig. 9a. Moreover, two vortices extending from the rear of the train are caused by the flow separation on the lateral sides of the trailing streamline of the train. Compared with the baseline model, the vortex structures in the wake region are much fewer, indicating that the presence of the bogies significantly affects the wake flow. Therefore, the current study designs two kinds of bogie cabin schemes based on the passive control method: (1) adding diversion grooves (Configuration 2) and (2) adding a spoiler (Configuration 3). For the baseline model (Configuration 1), small vortices exist when compared with the other configurations. Without any passive control devices, the incoming flow at the bottom could interact with the bogies and generate smaller vortices, as shown in Fig. 9b. However, for the model with passive control devices, when the airflow passes through the control devices, the direction of the airflow changes, and the interaction with the bogies is weakened. Therefore, the vortices decrease, as shown in Fig. 9c and d for the diversion grooves and spoiler, respectively.

Figure 10 shows the vorticity contour on planes at z = 0.2 m, y = 0 m, and z = 1.2 m for the different configurations. Configurations 2 and 3 have weaker vortex structures than the baseline model (Configuration 1), indicating that the adoption of passive control devices plays an important role in suppressing vortex structures around the train. Hence, the use of passive control devices may improve the aerodynamic

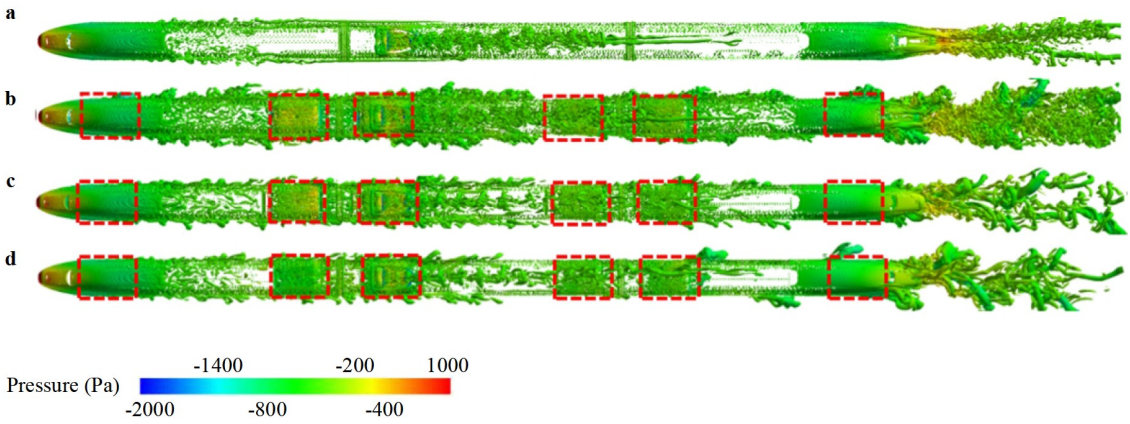

Figure 9 Instantaneous iso-surface of the Q-criterion (at Q = 1000). **a** Configuration 0: simplified model, **b** Configuration 1: baseline model, **c** Configuration 2: model with added diversion grooves, and **d** Configuration 3: model with added spoilers.

Table 3 Different configurations and their corresponding features

Configurations	Geometric features
Configuration 0	The baseline model without bogies
Configuration 1	The baseline model
Configuration 2	Model with adding diversion grooves
Configuration 3	Model with adding spoiler

performance of the train. Specifically, the greater the number of vortices around the train body, the greater the pressure fluctuation on the train body owing to the generation, attenuation, and shedding of vortices, and the stronger the unsteady flow on the train body surface. The aerodynamic noise of high-speed trains is mainly generated by dipole sound sources, which are caused by the variation in aerodynamic loads on the train surface. Thus, a close relationship exists between turbulent vortices and noise. The magnitude of the pressure fluctuation on the body surface is closely related to the far-field noise. To summarize, the flow field can reflect the noise to a certain extent, although further quantitative studies are still needed.

As seen in Table 4, the drag reductions and lift coefficients of each car achieved by the diversion grooves and spoiler are compared to quantitatively indicate the impacts of passive control devices on aerodynamic characteristics such as drag and lift. When compared with Configuration 1, both Configurations 2 and 3 perform better, as seen in Table 3. Spe-

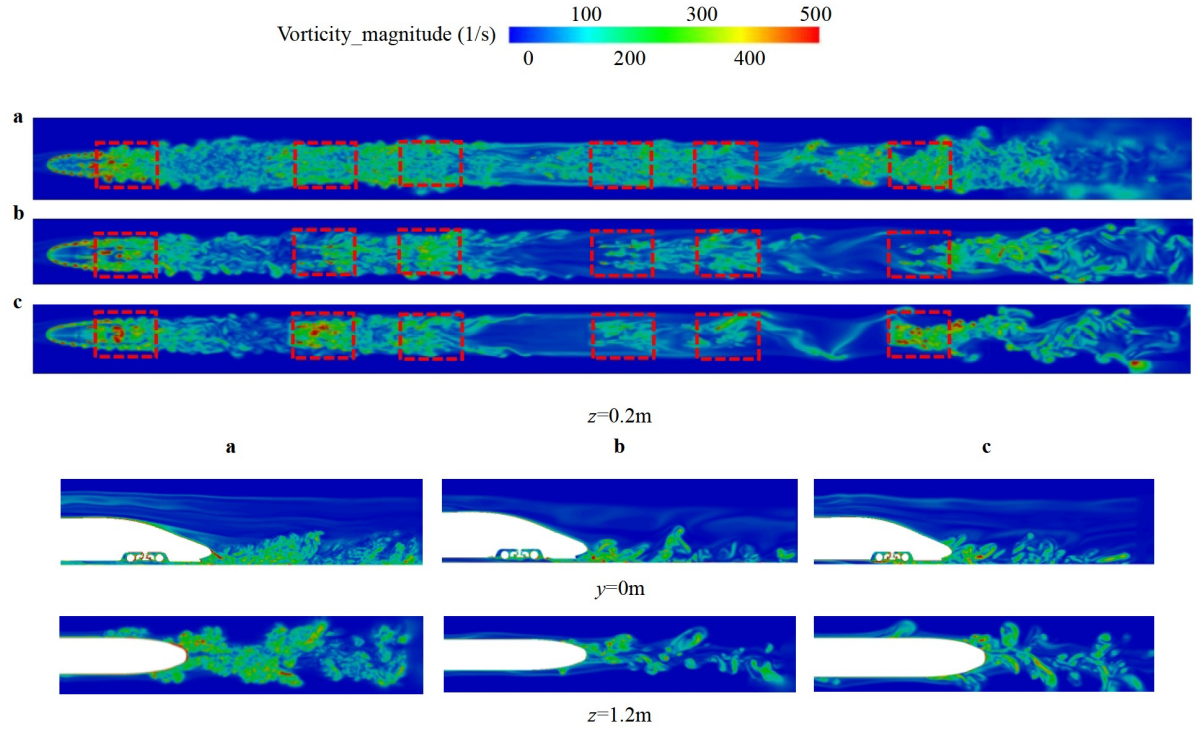

Figure 10 Vorticity magnitude (1/s) on plane z = 0.2 m, y = 0 m, and z = 1.2 m for **a** Configuration 1: baseline model with bogies, **b** Configuration 2: adding diversion grooves, and **c** Configuration 3: adding spoiler.

cifically, the total drag of Configuration 3 is reduced by 9.28%, and the lift coefficients in the tail car of Configuration 3 are also the lowest.

The velocity contours around four different bogies (bogies under the leading and trailing cars) for different configurations are given in Fig. 11 to highlight the differences in flow characteristics produced by passive control devices. When the airflow strikes the bogie, the airflow direction slightly deviates. However, due to the presence of the diversion devices, the air moves away from the wheels greatly. Consequently, the pressure drag on the wheels decreases significantly. The drop in the flow speed after installing the devices is more considerable in the area of the bogie's rear wheels, notably for Configuration 3. The flow speed near the ground decreases after adding the devices, especially when the spoiler is used. Flow separation is more likely to occur for the baseline shape as the boundary layer develops, resulting in higher pressure and friction resistance on the surface of the car body. Consequently, the drag coefficient increases. The position of the vertical lines designated at the front and rear positions of the bogie in Fig. 11 will be examined in the following sections by the velocity profiles along the vertical direction.

4.3 Effect of passive control devices on the slipstream

To understand the influence of the control devices on the flow field, the velocity profiles along the vertical direction at different locations are presented in Fig. 12. These locations refer to the locations mentioned previously and depicted in Fig. 11, and they are all just before and after the bogie. The air velocity remains zero at the top of the cabin, as shown by the velocity profiles. The velocity progressively increases as it approaches the ground until it reaches its maximum. It can be seen in Configuration 1 that without flow control devices, the flow accelerates significantly around the height of 0.1-0.15, indicating that the flow impinges more easily on the bogies. However, when passive control devices are used,

Table 4 Effect on drag and lift reductions for different passive control methods

Configuration	$C_{d,p}$	$C_{d,f}$	$C_{d,total}$	Head-Cl	Middle-Cl	Tail-Cl	ΔC_d (%)
1	0.2197	0.1111	0.3308	−0.1210	−0.0192	0.0799	–
2	0.1939	0.1089	0.3028	−0.1119	−0.0001	0.0631	−8.46
3	0.1911	0.1090	0.3001	−0.0868	−0.0208	0.0162	−9.28

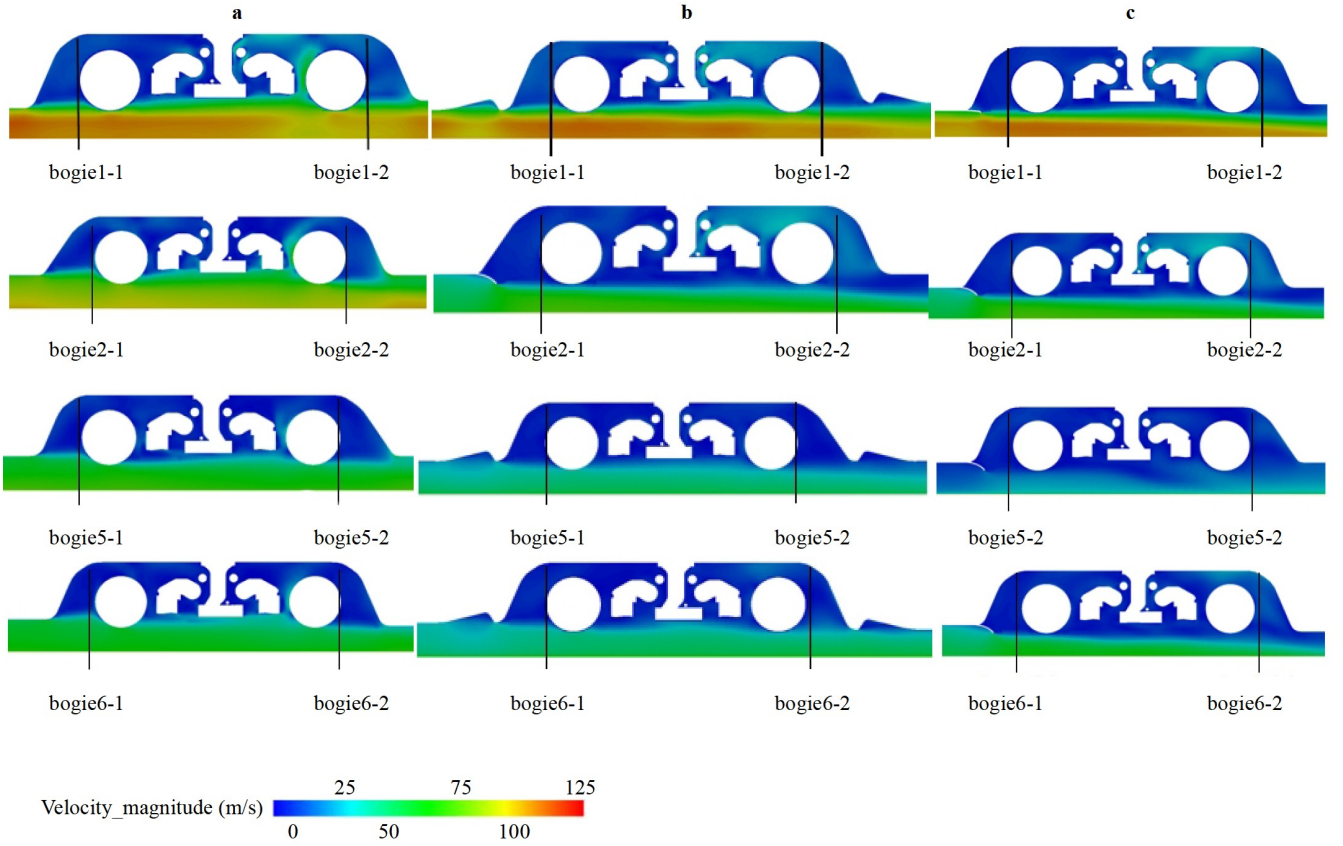

Figure 11 Velocity contours around bogies: **a** Configuration 1: baseline model, **b** Configuration 2: adding diversion grooves, and **c** Configuration 3: adding a spoiler.

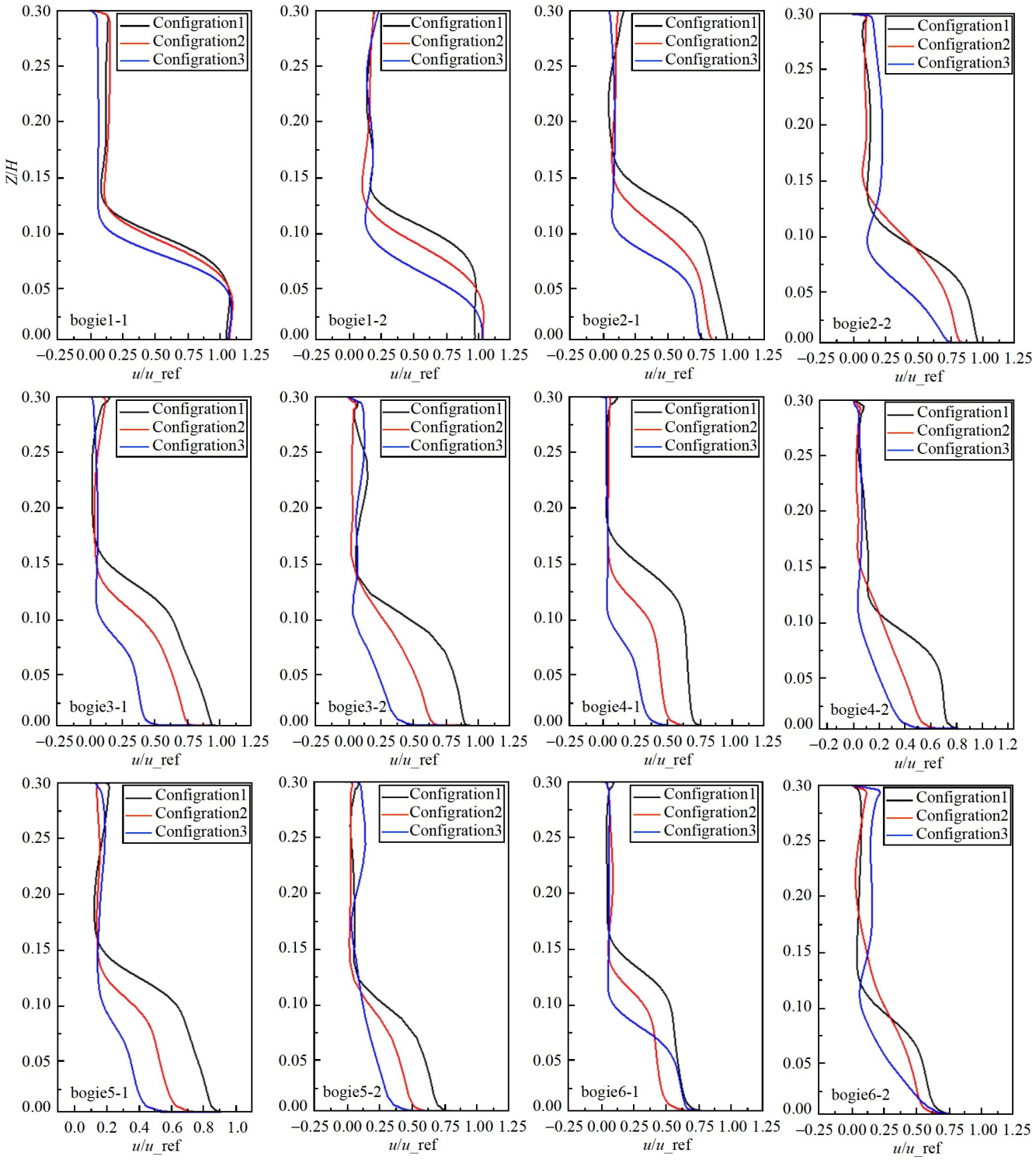

Figure 12 Velocity profiles at different locations for three configurations: Configuration 1: baseline model, Configuration 2: adding diversion grooves, and Configuration 3: adding a spoiler.

Configurations 2 and 3 show that the flow is disturbed greatly, and the accelerated flow is guided along the passive control devices downward obviously, which weakens the impingement impact on the bogies as expected.

Figure 13 compares the distributions of the time-averaged slipstream velocity along the monitoring lines at y = 3.0 and 4.0 m from the COT and 1.2 m above the ground. A sharp peak appears as the leading car passes by. After that, the peak decreases and is followed by a slipstream velocity recovery in the flow development region. In this region, the values of the time-averaged slipstream velocity obtained from Configuration 3 are higher than those from Configurations 1 and

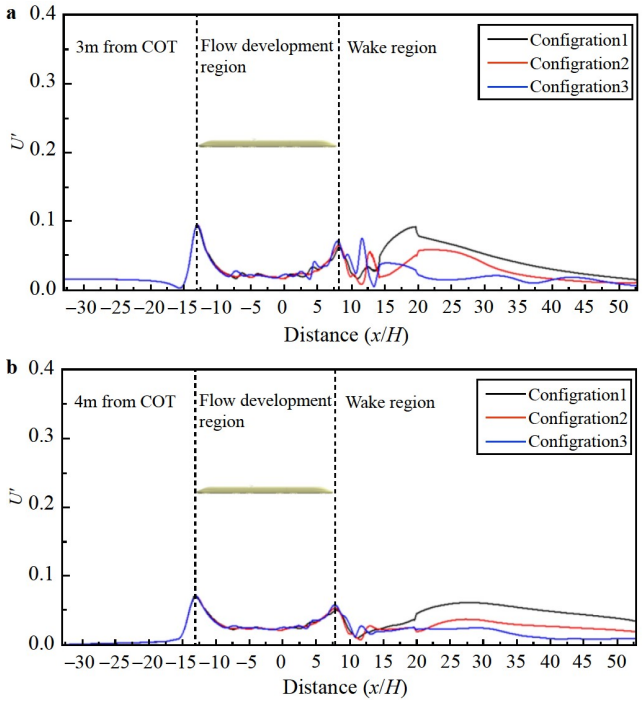

Figure 13 Comparison of time-averaged slipstream velocity distributions along monitoring lines at distances of **a** 3.0 m and **b** 4.0 m from COT for the three configurations. Configuration 1: baseline model, Configuration 2: adding diversion grooves, and Configuration 3: adding a spoiler.

2. Moreover, it is found that the values of the time-averaged slipstream velocity obtained from Configuration 2 are stronger than those from Configuration 1 at some monitoring points. These phenomena could be explained by the fact that Configuration 3 adds the spoiler at the front of the bogie cabin, thereby reducing the flow area from the bottom of the vehicle body to the downstream. Thus, the flow speed is accelerated, and the flow velocity in the surrounding area increases. In Configuration 2, the impact of the fluid flowing out of the deflector on the bogie is weakened by the addition of the deflector, as shown in Fig. 10. In addition, the extreme value of the time-averaged slipstream velocity appears in the wake region. The values of the time-averaged slipstream velocity in Configuration 1 are higher than those in Configurations 2 and 3 in the wake region. After the control devices are added, the value is reduced compared with Configuration 1. This reduction is because the complex structure of the bogies in Configuration 1 is directly exposed to the incoming flow, resulting in a higher turbulence level. In Configurations 2 and 3, the passive control designs can reduce the scale of vorticity level in the wake, thus weakening the velocity magnitude in the wake.

To understand the flow phenomena in the wake region, cross-sectional vortex structures generated by the three configurations at different distances from the rear of the vehicle, i.e., H, $2H$, and $3H$, are shown in Fig. 14. For Configuration 1, the vortex cores are nearly symmetrical, as shown in Fig. 14a. For Configurations 2 and 3, with the

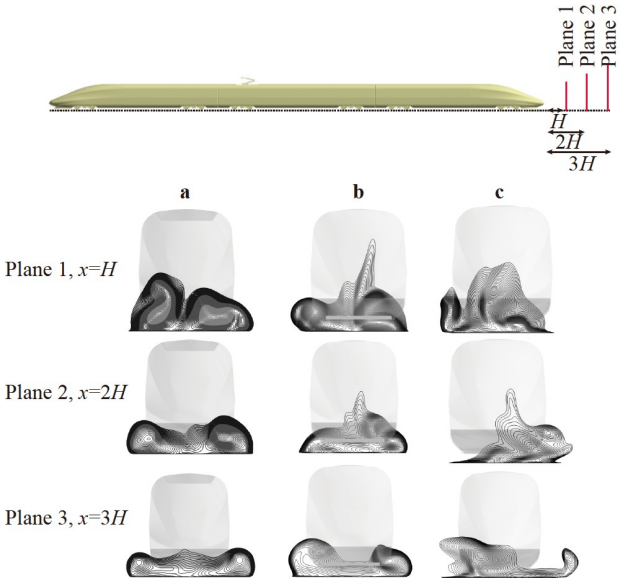

Figure 14 Comparison of cross-sectional vortex structures between different configurations at vertical planes from the trailing nose in the wake region with distances of $x = 1H$, $x = 2H$, and $x = 3H$. **a** Configuration 1: baseline model, **b** Configuration 2: adding diversion grooves, and **c** Configuration 3: adding a spoiler.

inclusion of the passive control devices, the position of the vortex cores is alternately distributed, especially when the spoiler is used. The rear vortex forms the same shedding trend as the Kármán vortex street, as shown in Fig. 14b and c, respectively. Moreover, the addition of passive control devices reduces the generation of turbulent structures. These devices can reduce the scale of the cross-sectional vortices and the streamwise vorticity level in the wake, thereby reducing the slipstream velocity distribution in the wake, as previously shown in Fig. 13.

4.4 Effect of passive control devices on aerodynamic noise

Here, the effects of passive control devices on aerodynamic noise are discussed. First, the root mean square (RMS) value of the surface pressure is provided. Then, the propagation of aerodynamic noise and its attenuation characteristics are studied.

4.4.1 RMS surface pressure

To evaluate the effects of the passive control devices on aerodynamic noise, the RMS surface pressure is first presented by the pressure fluctuation on the body surface. This pressure fluctuation is evaluated in decibels (dB), which can be determined using $L_p(\mathrm{dB}) = 10\log\left(P_{\mathrm{rms}}^2 / P_{\mathrm{ref}}^2\right)$, where P_{rms} is the RMS value of the pressure fluctuation, and P_{ref} is the reference sound pressure (2×10^{-5}) [43]. Figure 15 compares the RMS surface pressure distributions obtained from the three configurations at frequencies of 200 and

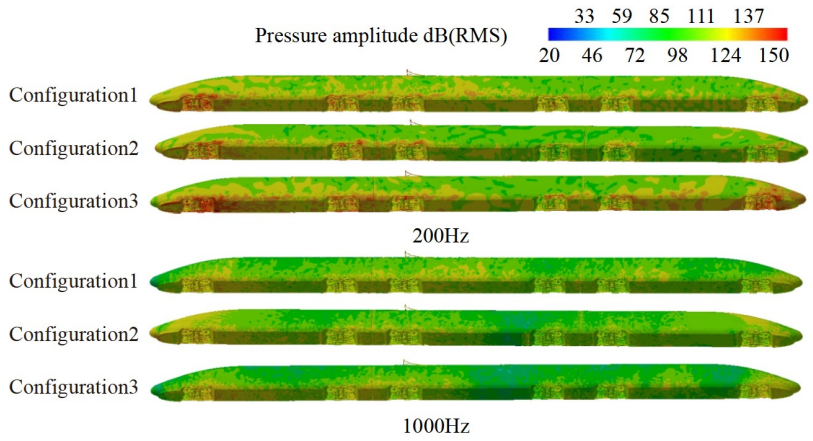

Figure 15 RMS surface pressure in decibels with reference sound pressure 2×10^{-5} Pa obtained from Configuration 1: baseline model, Configuration 2: adding diversion grooves, and Configuration 3: adding spoiler at frequencies of **a** 200 and **b** 1000 Hz.

1000 Hz.

Due to the slender shape of high-speed trains and airflow from front to back, the boundary layer becomes thicker, thus reducing the impact of airflow on the downstream structures. Therefore, the amplitude of the pressure fluctuations at the rear of the train is reduced. Moreover, it can be observed that along the direction of the incoming flow, the amplitude of the pressure fluctuations in the area around the bogies is higher than that in other areas of the train. This may be due to the complex structure of the bogie and its inclusion in the bogie cabin, which is similar to a cavity. These bogies collide with the incoming flow. Owing to the presence of the bogie cabin, the airflow interacts with the bogies in the bogie cabins, generating complicated vortices, as earlier shown in Figs. 8 and 9. Therefore, the amplitude of the pressure fluctuations in the region around the bogies is higher. The highest amplitude of the pressure fluctuations for the three configurations is observed on the first bogie.

Although the amplitude distributions of the pressure fluctuations obtained in the three configurations on the train surfaces are different at the two frequencies, the largest amplitudes are always located in the first car, as shown in Fig. 15. However, the amplitude decreases when the frequency increases from 200 to 1000 Hz. Zhang et al. [26] reported a phenomenon whereby the maximum aerodynamic pressure fluctuation decreases as the frequency increases. Among the three configurations, Configuration 1 has the largest area with a high amplitude of pressure fluctuations at both frequencies. At 1000 Hz, the area with low amplitudes in Configuration 3 is larger than that of other configurations. Compared with Configurations 1 and 2, the area with low amplitudes of Configuration 2 is larger.

4.4.2 Aerodynamic noise propagation and attenuation characteristics

To study the propagation of aerodynamic noise and the characteristics of noise attenuation from the high-speed train, the SPL generated by the three configurations is investigated in the range of −60 m to 60 m along the train-body direction, at 25 m from the central axis of the track and 3.5 m above the ground. The monitoring points are placed every 10 m, and 12 monitoring points are selected to investigate the noise characteristics. Figure 16 shows the sound spectra of four points at the positions of −60 m, −20 m, 20 m, and 60 m.

Generally, noise at low frequencies (< 300 Hz) contributes the most to the overall sound pressure level. The SPL distributions within 300 Hz are compared, and it can be observed that at 60 m, the SPL of Configuration 1 is the highest for most of the frequencies within 300 Hz. At −20 m, the maximum amplitude of configuration 1 exceeds that of the other two configurations. At 20 m, the peak values of the three configurations are very close, and the overall amplitude of Configuration 3 is the lowest. At 60 m, Configuration 2 gives lower SPLs than the other two configurations.

To complete the investigation on sound propagation, Fig. 17 shows the OASPL along the x-direction at $y = 25$ m. The noise amplitude increases along the train body. Furthermore, the noise is reduced after the passive control devices are used, especially when the spoiler is added, as the noise amplitude obtained from Configuration 3 is the lowest, indicating that the noise reduction effect of the spoiler is the best. Therefore, it can be concluded that the presence of diversion grooves and a spoiler can play an important role in reducing aerodynamic noise in the far field and that the use of passive control devices can be considered for real operations in high-speed trains.

5. Conclusion

This study presents the effects of different passive control methods, i.e., spoilers and diversion grooves on the slipstream, drag, and aerodynamic noise of high-speed trains using IDDES and acoustic FEM. Numerical simulations are

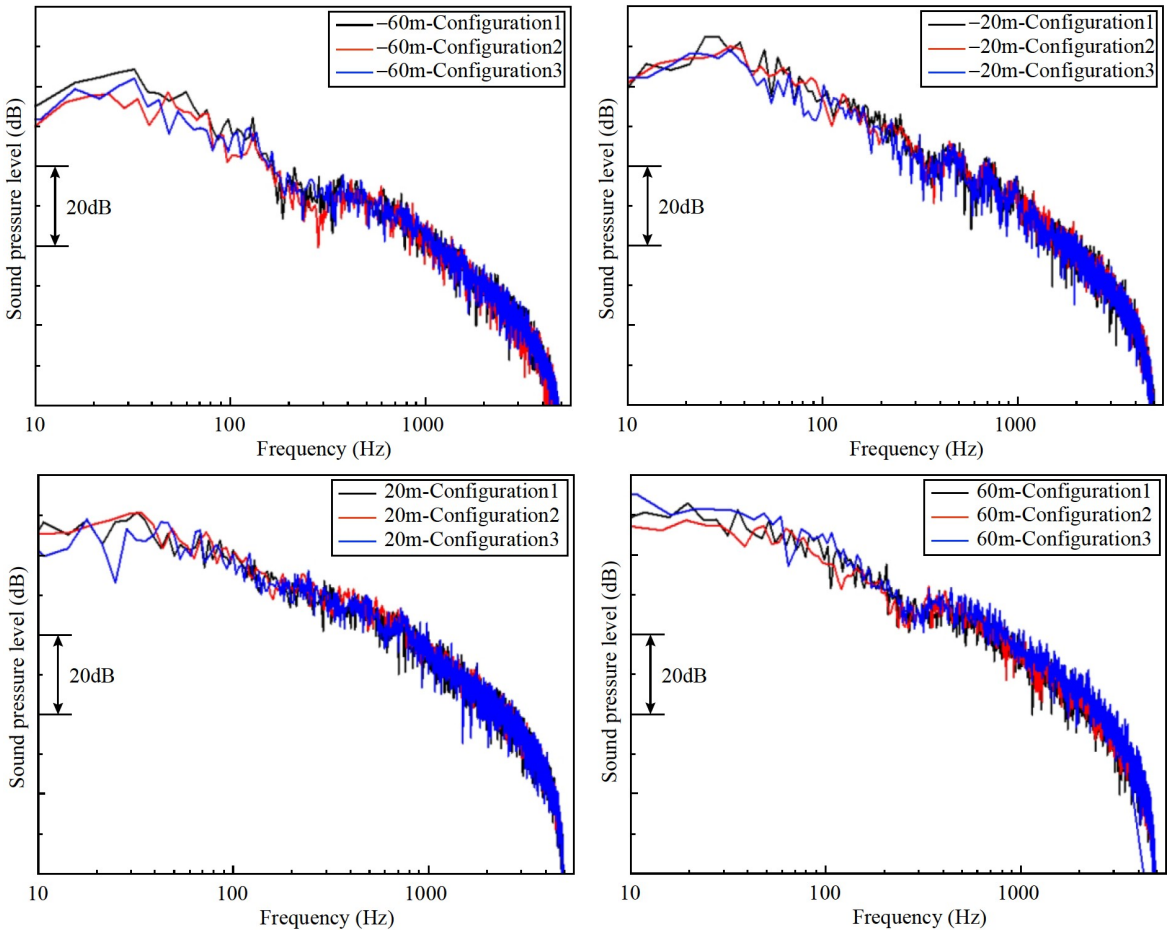

Figure 16 Sound spectra of four points along the x-direction. x = −60, −20, 20, and 60 m of Configuration 1: baseline model, Configuration 2: adding diversion grooves, and Configuration 3: adding a spoiler.

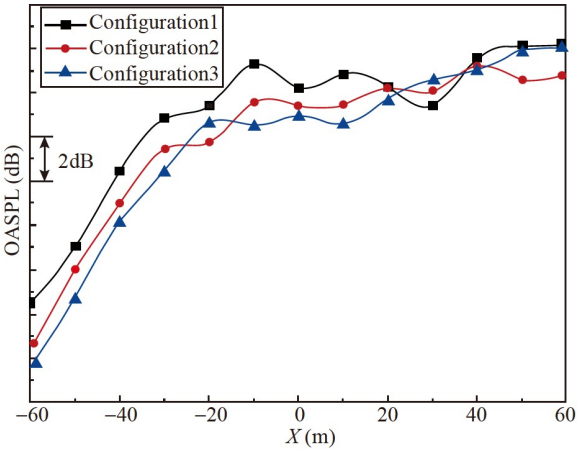

Figure 17 OASPL along the x-direction at y = 25 m, z = 3.5 m of Configuration 1: baseline model, Configuration 2: adding diversion grooves, and Configuration 3: adding a spoiler.

conducted to study the aerodynamic and noise characteristics of the train at $Re = 2.3 \times 10^7$. The accuracy of the numerical method is validated using experimental results from moving model experiments, and the following conclusions can be drawn from the results.

The passive control devices have a dominant effect on the slipstream pressure and velocity distribution around the train. Compared with the bogies exposed to the incoming airflow, the interaction between the incoming airflow and the bogies is weakened in the model with the passive control devices, and the vortices decrease. The incoming velocity in the bogie cabin is reduced. Moreover, it reduces the height and width of the wake flow, including the streamwise vorticity level in the wake, thereby lowering the slipstream velocity distribution in the wake. Therefore, adding control devices is recommended to improve the safety and comfort of passengers.

Both control devices reduce aerodynamic drag and noise in the far field. The control devices proposed herein play a key role in reducing drag, slipstream, and noise, which will shed light on the design of bogie cabins.

Additionally, some remarks should be given here. Several problems can be further explored about the passive control measures adopted herein. The design of the spoilers and diversion grooves can be considered in various ways. For the spoiler, the distance between the placement of the spoiler and the front end of the bogie cabin, as well as the width and

curvature of the spoiler itself, can be treated as design variables to consider their impact on the aerodynamic performance and noise characteristics of the train. In addition, when adding the diversion grooves in the front of the bogie cabin, the width, depth, and angle of the triangular cross-section of the diversion grooves, as well as the distance between the rear end of the grooves and the front end of the bogie cabin, can all be considered design variables. These variables may be key factors that affect the flow field and result in severe variation in the drag and noise of high-speed trains. Even though this study excludes the influence of the configuration design of passive control devices, further parametric studies of the variables will be conducted to improve the aerodynamic and noise performance of high-speed trains.

Acknowledgements *This work was supported by the Youth Innovation Promotion Association of the Chinese Academy of Sciences (Grant No. 2019020), the Strategic Priority Research Program of the Chinese Academy of Sciences (Class B) (Grant No. XDB22020000), and the Informatization Plan of the Chinese Academy of Sciences (Grant No. XXH13506-204).*

1 R. S. Raghunathan, H. D. Kim, and T. Setoguchi, Aerodynamics of high-speed railway train, Prog. Aerospace Sci. **38**, 469 (2002).
2 A. D. Vakili, G. A. Givogue, and W. L. Fowler, in An experimental investigation of 2-D cylinders affecting supersonic cavity flow: Proceedings of the 29th AIAA Applied Aerodynamics Conference, Honolulu, 2011.
3 G. J. Milne, C. C. Thieman, and A. Vakili, in An experimental investigation of supersonic cavity flow control with vertical cylinders: Proceedings of the 43rd Fluid Dynamics Conference, San Diego, 2013.
4 A. Miyako, and Y. Yamamoto, in Investigation of running resistance of high speed trains: Proceedings of the World Congress on Railway Research (WCRR, Florence, 1997), pp. 577-579.
5 C. Baker, The flow around high speed trains, J. Wind Eng. Industrial Aerodyn. **98**, 277 (2010).
6 A. Ido, S. Saitou, K. Nkakade, and S. Likura, in Study on underfloor flow to reduce ballast flying phenomena: Proceedings of the 8th World Congress on Railway Research, Seoul, 2008.
7 S. Wang, D. Burton, A. Herbst, J. Sheridan, and M. C. Thompson, The effect of bogies on high-speed train slipstream and wake, J. Fluids Struct. **83**, 471 (2018).
8 Z. X. Huang, L. Chen, and K. Jiang, Wind tunnel test of air drag reduction schemes of high-speed trains, J. China Railw. Soc. **34**, 16 (2012).
9 H. J. Kaltenbach, I. A. Portillo, and M. Schober, in A generic train-under floor experiment for CFD validation: Proceedings of BBAA VI International Colloquium on Bluff Bodies Aerodynamics and Applications (Milano, 2008), pp. 20-24.
10 Z. G. Yang, and Z. Gao, Numerical analysis on influence on aerodynamic performance of high-speed train caused by installation of skirt plates, Comput. Aided Eng. **3**, 16 (2010).
11 H. F. Wang, K. H. Yih, G. H. Lee, and S. L. Huang, Synthesis and characterization of the first doubly-bridged N, N-dimethylthiocarbamoyl metal complex: Crystal structure of $[Mo(Cl)(CO)_2(PPh_3)]_2(\eta^1{:}\eta^2{:}\mu\text{-}SCNMe_2)_2$, J. Chin. Chem. Soc. **58**, 15 (2011).
12 X. H. Zheng, J. Y. Zhang, and W. H. Zhang, Numerical simulation of aerodynamic drag for high speed train bogies, J. Traffic Transp. Eng. **11**, 45 (2011).
13 Y. Chen, Z. Gao, and Y. G. Wang, Effect of underbody guide plate forms on aerodynamic drag of high-speed train, Comp. Aided Eng. **25**, 29 (2016).
14 J. Wang, G. Minelli, T. Dong, G. Chen, and S. Krajnović, The effect of bogie fairings on the slipstream and wake flow of a high-speed train: An IDDES study, J. Wind Eng. Indust. Aerodyn. **191**, 183 (2019).
15 Z. Sun, Y. Yao, Y. Yang, G. Yang, and D. Guo, Overview of the research progress on aerodynamic noise of high-speed trains in China (in Chinese), Acta Aerodyn. Sin. **36**, 385 (2018).
16 J. Zhang, and C. Zhu, Far field noise contribution radiated from aerodynamic noise source of high speed train, China Railw. Sci. **40**, 115 (2019).
17 S. S. Ding, D. W. Chen, and J. L. Liu, Research development and prospect of China high speed train, Chin. J. Theor. Appl. Mech. **53**, 35 (2021).
18 R. D. Liu, C. S. He, and Y. L. Li, Numerical simulation analysis of aerodynamic noise source intensity and distribution characteristics of high speed train, Railw. Energy Conserv. Environ. Prot. Saf. Health **10**, 1 (2020).
19 D. Z. Wang, and J. M. Ge, Noise characteristics in different bogies areas during high speed train operation, J. Traffic Transp. Eng. **20**, 174 (2020).
20 J. W. Shi, H. Wang, and X. Z. Sheng, Aerodynamic noise characteristics of bogies at 400 km/h, Noise Vib. Control **40**, 125 (2020).
21 D. J. Thompson, E. Latorre Iglesias, X. Liu, J. Zhu, and Z. Hu, Recent developments in the prediction and control of aerodynamic noise from high-speed trains, Int. J. Rail Transp. **3**, 119 (2015).
22 D. J. Thompson, Railway Noise and Vibration: Mechanisms, Modeling and Means of Control (Elsevier, Oxford, 2008).
23 N. Frémion, N. Vincent, M. Jacob, G. Robert, A. Louisot, and S. Guerrand, Aerodynamic noise radiated by the intercoach spacing and the bogie of a high-speed train, J. Sound Vib. **231**, 577 (2000).
24 A. Torii, and J. Ito, Development of the series 700 Shinkansen train-set (Improvement of noise level), jpn. Railw. Eng. **14**, 16 (2000).
25 S. Huang, M. Z. Yang, Z. W. Li, and G. Xu, Aerodynamic noise numerical simulation and noise reduction of high speed train bogie section, J. Cent. S. Univ. **42**, 3899 (2011).
26 Y. Zhang, J. Zhang, T. Li, and L. Zhang, Numerical research on aerodynamic noise of trailer bogie, J. Mech. Eng. **52**, 106 (2016).
27 J. Y. Zhu, L. H. Ren, and Z. Y. Lei, Effective of bogie cavity on flow and flow-induced noise behavior around high-speed train bogie region, J. Tongji Univ. (Nat. Sci.) **46**, 1556 (2018).
28 A. Lauterbach, K. Ehrenfried, S. Loose, and C. Wagner, Microphone array wind tunnel measurements of Reynolds number effects in high-speed train aeroacoustics, Int. J. Aeroacoustics **11**, 411 (2012).
29 E. Latorre Iglesias, D. J. Thompson, M. Smith, T. Kitagawa, and N. Yamazaki, Anechoic wind tunnel tests on high-speed train bogie aerodynamic noise, Int. J. Rail Transp. **5**, 87 (2016).
30 Z. Yang, Z. Gao, Y. Chen, and Y. Wang, Numerical analysis on influence on aerodynamic performance of high-speed train caused by installation of skirt plates. Comp. Aided Eng. **19**, 16 (2010).
31 P. R. Spalart, W. H. Jou, M. Strelets, and S. Allmaras, Comments on the feasibility of LES for wings, and on a hybrid RANS/LES approach, in: Advances in DNS/LES (Grayden Press, Columbus, 1997).
32 P. R. Spalart, S. Deck, M. L. Shur, K. D. Squires, M. K. Strelets, and A. Travin, A new version of detached-eddy simulation, resistant to ambiguous grid densities, Theoret. Comput. Fluid Dyn. **20**, 181 (2006).
33 F. R. Menter, Two-equation eddy-viscosity turbulence models for engineering applications, AIAA J. **32**, 1598 (1994).
34 M. L. Shur, P. R. Spalart, M. K. Strelets, and A. K. Travin, A hybrid RANS-LES approach with delayed-DES and wall-modelled LES capabilities, Int. J. Heat Fluid Flow **29**, 1638 (2008).
35 T. Dong, G. Minelli, J. Wang, X. Liang, and S. Krajnović, The effect of reducing the underbody clearance on the aerodynamics of a high-speed train, J. Wind Eng. Ind. Aerodyn. **204**, 104249 (2020).
36 J. Niu, D. Zhou, T. Liu, and X. Liang, Numerical simulation of aerodynamic performance of a couple multiple units high-speed train, Veh. Syst. Dyn. **55**, 681 (2017).
37 C. Xia, H. Wang, X. Shan, Z. Yang, and Q. Li, Effects of ground

configurations on the slipstream and near wake of a high-speed train, J. Wind Eng. Ind. Aerodyn. **168**, 177 (2017).
38 M. S. Gritskevich, A. V. Garbaruk, J. Schütze, and F. R. Menter, Development of DDES and IDDES formulations for the *k*-*ω* shear stress transport model, Flow Turbul. Combust **88**, 431 (2012).
39 A. Fioravanti, G. Lenzi, G. Vichi, G. Ferrara, S. Ricci, and L. Bagnoli, Assessment and experimental validation of a 3D acoustic model of a motorcycle muffler, SAE Int. J. Engines **8**, 266 (2015).
40 Y. Yao, Z. Sun, G. Yang, W. Liu, and P. Prapamonthon, Analysis of aerodynamic noise characteristics of high-speed train pantograph with different installation bases, Appl. Sci. **9**, 2332 (2019).
41 Y. Yao, Z. Sun, W. Liu, and G. Yang, Analysis of aerodynamic noise characteristics of pantograph in high speed train (in Chinese). Acta Scientiarum Naturalium Universitatis Pekinensis **56**, 385 (2020).
42 C. Cong, X. Deng, and M. Mao, Advances in complex low speed flow around a prolate spheroid (in Chinese), Adv. Mech. **51**, 467 (2021).
43 Q. Zhang, Fundamentals of Aeroacoustics (National Defense Industry Press, Beijing, 2012).

基于被动控制装置的高速列车转向架区域气动优化

姚永芳, 孙振旭, 李桂波, 杨国伟, Prasert Prapamonthon, 郭易, 王梦莹

摘要 高速列车转向架是重要的气动阻力和噪声来源, 这两者都会对高速列车气动性能和乘客的舒适性带来不利影响. 在本研究中, 将被动控制的方法应用于高速列车转向架舱的设计, 以改善其气动性能. 本研究引入了两种被动控制措施, 即加装扰流片和在转向架舱附近设置导流槽. 本文采用改进的延迟分离涡模拟(IDDES)和声学有限元法(FEM), 对高速列车不同被动控制策略下的气动特性和气动声学特性进行了数值研究, 分析并讨论了被动控制装置对减阻、周围气流和气动噪声特性的影响. 研究结果表明, 被动控制装置对列车周围气流有重要影响. 列车前半部分脉动压力幅值高于后半部分. 无论是否加装被动控制装置, 第一个转向架处的声压振幅都是最大的. 对于远场区域, 在转向架舱前安装扰流片和放置导流槽可以明显降低气动阻力和噪声. 因此, 如本研究所示, 采用被动控制方法来改善高速列车气动特性和噪声特性是一种可行的选择.